Delft University of Technology

Early-age creep of 3D printable mortar
Experiments and analytical modelling

Chang, Ze; Liang, Minfei; Xu, Yading; Wan, Zhi; Schlangen, Erik; Šavija, Branko

Important note
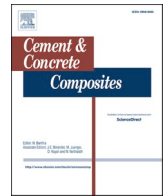To cite this publication, please use the final published version (if applicable).
Please check the document version above.

Early-age creep of 3D printable mortar: Experiments and analytical modelling

Ze Chang, Minfei Liang [*], Yading Xu, Zhi Wan, Erik Schlangen, Branko Šavija

Microlab, Faculty of Civil Engineering and Geosciences, Delft University of Technology, 2628 CN, Delft, the Netherlands

A R T I C L E   I N F O

A B S T R A C T

In this study, an experimental setup to characterize the early-age creep of 3D printable mortar was proposed. The testing protocol comprises quasi-static compressive loading-unloading cycles, with 180-s holding periods in between. An analytical model based on a double power law was used to predict creep compliance with hardening time and loading duration as inputs. Subsequently, this analytical model was validated by comparison to uniaxial compression tests in which loading is increased incrementally, i.e., in steps, showing a good quantitative agreement. Minor differences between the two results were noted, most notably at the beginning of the test. This is because the determination of creep compliance for 3D printable mortar at fresh stage depends on the load level. In the end, the volumetric strain of tested samples from uniaxial compressive test is used to explain why the compressive loading affects the creep deformation.

1. Introduction

Addictive manufacturing (AM) is an emerging digital fabrication technique which can revolutionize the construction industry by producing high-quality building elements while requiring less labour and time compared to traditional concrete [1,2]. The most widely-used AM technology in the construction sector is extrusion-based 3D concrete printing (3DCP) [3]. Not only can 3DCP do away with the need for traditional moulds, thereby decreasing post-construction waste, it can also significantly speed up the manufacturing process and yield geometrically complicated, non-standard structural elements rather than rectilinear shapes [4,5].

Based on the acknowledged feasibility of 3DCP in the construction industry, there have also been several large-scale building projects over the past several years [6,7]. The Eindhoven University of Technology has completed a bicycle bridge in Gemert for public use through 3DCP [8]. Using their own developed high-thixotropy 3D printing material, Zhang et al. constructed a bus station in situ without the need of formwork [6]. A more complex geometric cellular structure has been printed by a cooperative research group from the University of Southern Denmark and Politecnico di Milano [9]. These projects demonstrate the application of 3DCP in the construction sector. Full industrial adoption, however, is still a long way off. A number of problems in the field of material science and mechanical analysis still need to be resolved.

In 3DCP, the cementitious materials are extruded from the nozzle and placed in the printed structure to create layers composed of a computer-designed geometry. After deposition, the material should be stiff enough to retain its shape and avoid collapse or buckling under self-weight and the gravitational loading from subsequent printing segments. This is defined as buildability performance [10–13]. To complete the printing process and ensure optimal performance for structural components or large-scale projects, excellent buildability is what we want to achieve. However, this performance is co-determined by several factors, consisting of the material properties, designed geometry and the printing scheme. Therefore, it is difficult to accurately predict the structural deformation during printing process. Such an issue is associated with early-age mechanical behaviour and there is limited knowledge in this field.

From pumping to deposition process at the fresh stage, 3D printed materials generally act as visco-elastic materials [9,10]. The viscoelasticity theory, which combines the viscous and elastic characteristics, can be used to explain how viscoelastic materials react [14]. To assess the elastic material behaviour, several testing techniques, including the unconfined uniaxial compression test [13,15–17], direct shear test [18], rotational rheometer [5,19], and ultrasonic wave transmission test have been used [20]. These techniques allow for the experimental derivation

of the green strength, yield stress, and pulse velocity, providing the fundamental material characteristics related to elastic and plastic deformation for structural deformation prediction. However, apart from these, there is an additional issue to be considered: the time-dependent structural deformation during the printing process. The layer-by-layer deposition process induces progressive compression in the printed filaments. Because of this, there is delayed deformation throughout the automated process, which can reduce the precision of printing or potentially cause structural failure. This type of delayed deformation occurs during the printing process and consists of basic creep, autogenous shrinkage, plastic shrinkage, and the consolidation settlement under compressive load. Since this delayed deformation certainly continues to increase over time under constant compressive loading for cementitious materials at fresh stage, the term 'early-age creep' is utilized to define this delayed behaviour.

In order to appropriately predict structural deformation, it is crucial to characterize the early-age creep behaviour of 3D printable materials at fresh stage. However, not many studies are available in the published literature even with conventional cementitious materials. The limited research demonstrates the feasibility of testing early-age creep by means of compressive tests [21,22], rheological tests [23,24] and ultrasonic tests [24,25]. The 3D printable materials differ from conventional cementitious materials in several aspects: (1) high past volume; (2) low water to cement (w/c) ratio; (3) addition of viscosity-modifying agent (VMA) [26–28]. These features affect the visco-elastic properties of 3D printable materials in their fresh state; for example, the high paste volume will make shrinkage and creep more pronounced [2]. Moreover, the layer-by-layer extrusion process may result in increased porosity compared to casting [29]. This creates more free space for water movement and results in higher creep [30]. Thus, understanding the early-age creep behaviour of the cementitious materials used in the 3DCP is crucial.

Further explorations about the early-age behaviour of 3D printable materials come from uniaxial compression tests conducted by Esposito et al. [23] and rheological tests performed by Chen et al. [31]. Rheological tests are more appropriate for quantifying the intrinsic early-age creep behaviour of cementitious materials since they can apply a very small shear force to particles within the elastic domain. A basic creep behaviour can therefore be derived. However, compression tests, on the other hand, can account for the influence of internal pores, the consolidation settlement due to the compressive loading, and environmental conditions on the final structural deformation, which is more consistent with printing trials. Esposito et al. [23] experimentally quantified early-age creep, and the results highlight that early-age creep accounts for a high ratio of the overall deformation of the tested sample. However, the effects of hydration, loading rate, and load level on the determination of creep compliance are not controlled during the testing process. In addition, the relationship between creep compliance with hardening time and loading duration is not known. Therefore, it is difficult to incorporate these experimental data into a numerical or analytical model and investigate their effect on structural deformation prediction and failure mode simulation.

To capture this kind of delayed deformation during the printing process, herein an early-age creep testing approach is proposed. Then, a relationship between early-age creep and printing time using analytical modelling is established and experimentally validated. Given that the total deformation is what is observed during printing process, this research, therefore, does not distinguish the contribution of each factor (i.e., autogenous shrinkage, drying shrinkage, basic creep and consolidation settlement) to the result. Thus, the proportion of each factor and their influence mechanism on the final deformation is outside of the scope of this study. This study characterizes the early-age creep of 3D printable materials, and experimental results are used to calibrate the creep compliance surface. With the loading history as input, this analytical model can predict the creep behaviour of the printed structure. However, the loading history of printed segments is codetermined

by the loading path and direction in 3DCP. The creep loading that is applied to the printed segment includes both its own weight and gravitational loading from subsequent printed layers. The main contribution of this study is the development of an analytical model that can be used to characterize the creep behavior of cementitious materials. The impact of loading direction and path on creep evolution will be studied in further research.

In this work, a self-designed experimental setup was proposed to characterize the early-age elastic and creep behaviour of 3D printable materials. The experimental results were then used to calibrate creep compliance surface using analytical modelling. This analytical model was validated by a 'compressive test', which mimics the loading condition of layer-by-layer extrusion process. The deviation between experimental results and analytical prediction was explained by a series of creep testing. In the end, the impact of load level on creep compliance was discussed via volumetric strain testing.

2. Materials and methods

2.1. 3D printable mortar

2.1.1. Mix design

Here, a self-developed 3D printable mortar was designed. To ensure the stiffness and strength after material deposition, a low w/c ratio is utilized for mix design [32,33]. The hydroxypropyl methylcellulose-based VMA is also added to the material to increase its viscosity in order to fulfil the criteria of pumpability [34]. After a series of trial-and-error, a mass ratio equal to 0.0024 between VMA and water is used in this study. Consequently, this material can be extruded from the nozzle without blocking it. The mix design is given in Table 1.

2.1.2. Pumpability and buildability test

The most straightforward method to assess the printability of cementitious materials is through laboratory tests for pumpability and buildability, as suggested by Le et al. [35]. Fig. 1 illustrates the extrusion-based mortar 3D printer utilized in this study. Fig. 2 indicates the nozzle dimension information in this used printer. This printer employs a gantry system and a 3D printed plastic nozzle is equipped on the gantry frame to move along in the x-y plane for printing. The print table can move along the z axis to raise or lower itself to the designed height. The effective printing size is 480 mm (l), 480 mm (w), and 500 mm (h), and the maximum volume of printing material in a batch is 1.5 L. It means the maximum amount of 3D printable mortar in a batch that could be printed at once is 1.5 L. A simple operation can be completed on the touch screen to change the printing process, and the printing parameters are fully controlled by the computer through WiFi in real time. This screen not only shows the detailed information about printing parameters, including the extrusion speed and nozzle speed, but also supplied the option to manually adjust the nozzle coordinate. In terms of printing procedure, the cementitious materials are manually filled into the ram extruder firmly to expel the entrapped air in printable materials. This RAM extruder is vertical type, which is made up of three parts, electrical machinery, a rotatable steel bar and a piston. Once it starts to work, the electrical machinery will drive the steel bar to rotate. The attached iron block can move down to push the piston. Thus, the fresh material will be pushed into the plastic hose and extruded on the print table. Table 2 describes the procedures for sample preparation and buildability test.

Fig. 3 (a) depicts mortar being extruded from the nozzle. It can be observed that mortar can be smoothly extruded from the nozzle without

Table 1
Compositions of 3D printable materials utilized in this study [kg/m^3].

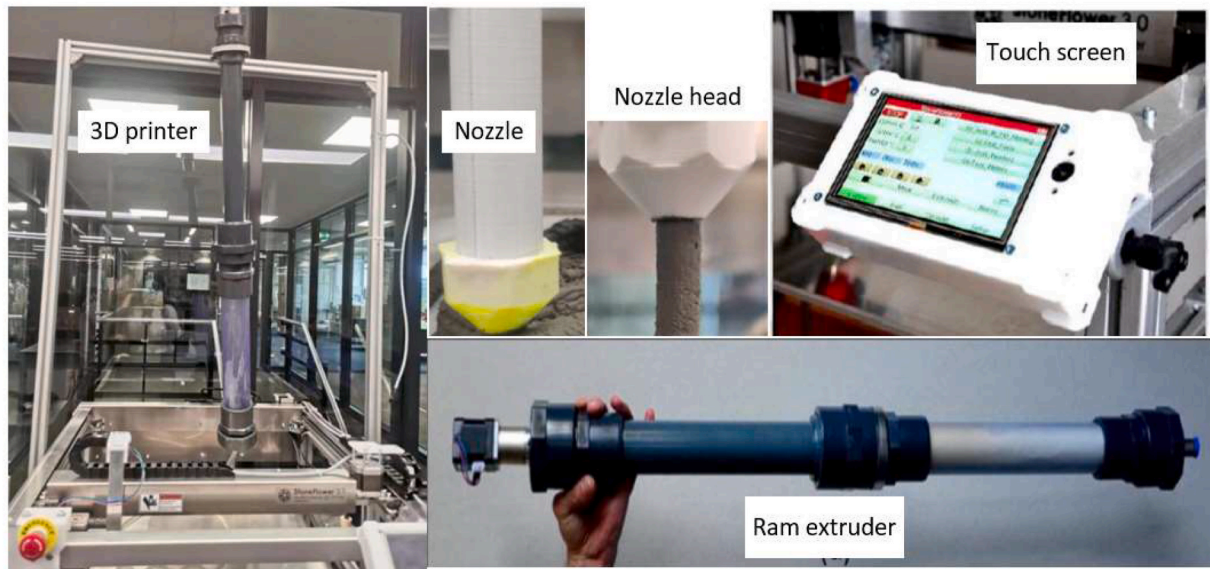| Cement	Water	VMA	Sand (0.01–0.02 mm)	w/c ratio	Cement type
1140	342	0.83	770	0.3	CEM I 42.5

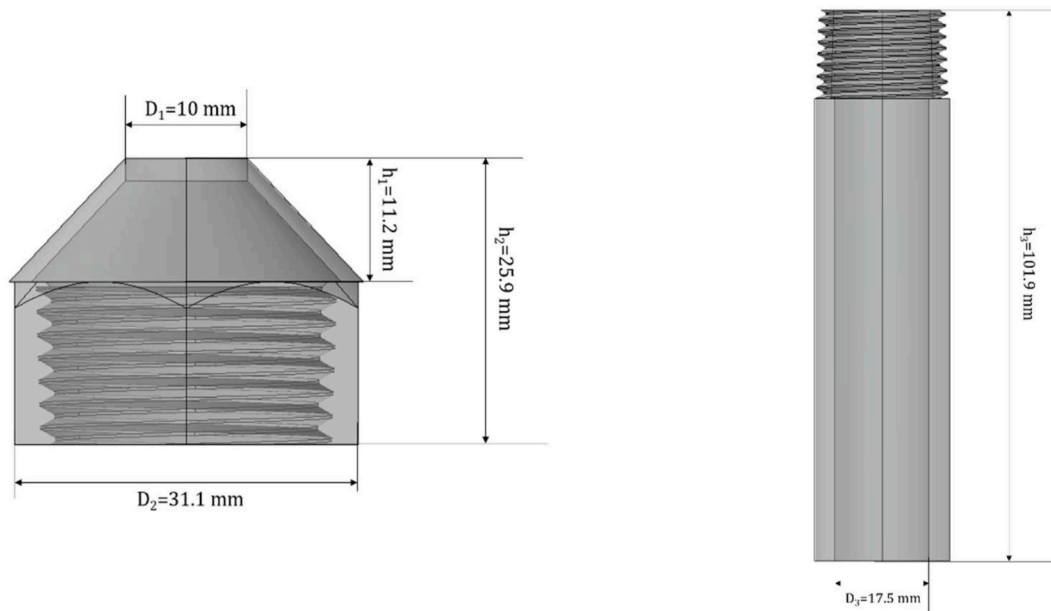**Fig. 1.** The 3D printer used in this study, and its components.

Fig. 2. A schematic diagram of nozzle dimensions information.

Table 2

Mixing procedures for the fresh mortar preparation and testing.

Time [min:s]	Mixing procedures
−2:00	Mix dry blends at low speed using a HOBART mixer
0:00	Add water during mixing
4:00	Stop, start to fill the barrel of the printer
4:00–20:00	Preparation before printing
20:00	Start printing

blockage, which demonstrates its good pumpability. In terms of the printing tests, the printed material preparation includes mixing and filling in the tube, which takes around 15 min in total. Subsequently, the prepared materials are installed on the printed machine and start to be printed. The time moment for material extruded is around 20 min after water adding. Then, the buildability of this material is evaluated by printing a hollow cylinder geometry and a free wall structure. After 20

layers of deposition, the hollow cylinder geometry with a 150 mm diameter and 6 mm layer height was successfully produced in around 20 min, as illustrated in Fig. 3 (b). The critical printing height of the free wall structure was then investigated in the second test, as shown in Fig. 3 (c). This wall structure, composed of extruded layers with 15 mm width, 4 mm thickness and 350 mm length, failed due to the out-of-plane displacement (i.e., elastic buckling failure mode) at 34 layers. A suitable pumpability and buildability performance can be observed through these three tests. Then, further experimental programs on early-age material characteristics, consisting of green strength and creep behaviour, will be introduced.

2.2. Experimental methods

Cement paste generally plays a significant influence in the creep of mortar and concrete [22]. Creep of Portland cement paste is highly
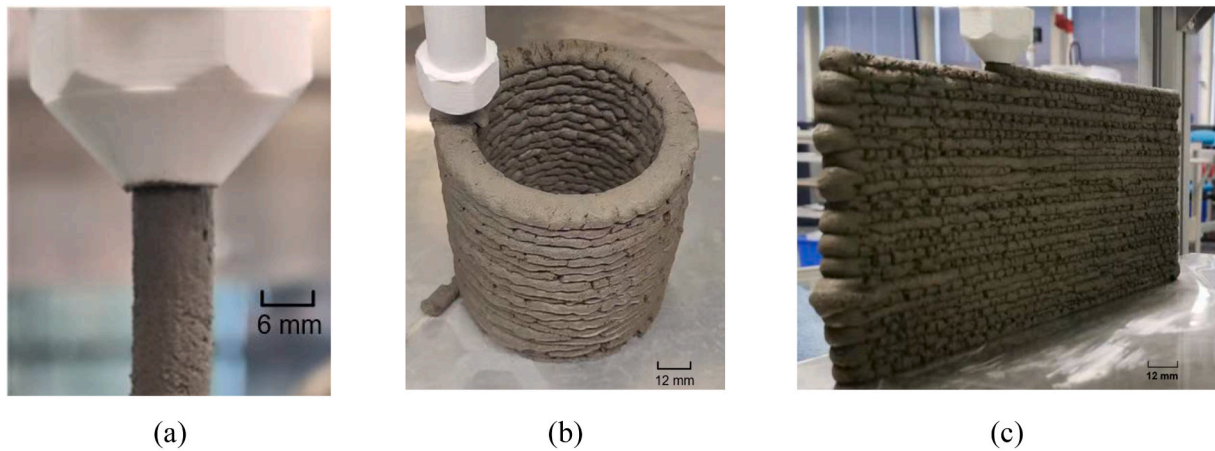
(a)   (b)   (c)

Fig. 3. Printability quantification of designed material (a) pumpability test (b) buildability test: hollow cylinder structure (b) buildability test: wall structure.

co-determined by the porosity and calcium silicate hydrates (C–S–H). Macroscale experiments to evaluate the creep evolution of hardened cementitious materials usually adopt a low creep loading, below 30% or 45% of compressive strength [36,37], which aims to exclude the influence of damage on creep measurement. This load ratio is generally adopted for creep analysis of hardened cementitious material; however, it might need to be revised for cementitious materials at fresh stage.

2.2.1. Green strength test

The 'green strength' which allows fresh concrete to carry the self-weight immediately after mixing or compacting, is attributed to a combined inter particle friction, and cohesion [15]. In this research, the green strength is uniaxial compressive strength of cementitious materials at the fresh stage. The green strength tests were carried out to measure the compressive strength of 3D printable material in the fresh stage [15]. The displacement-controlled compression tests were
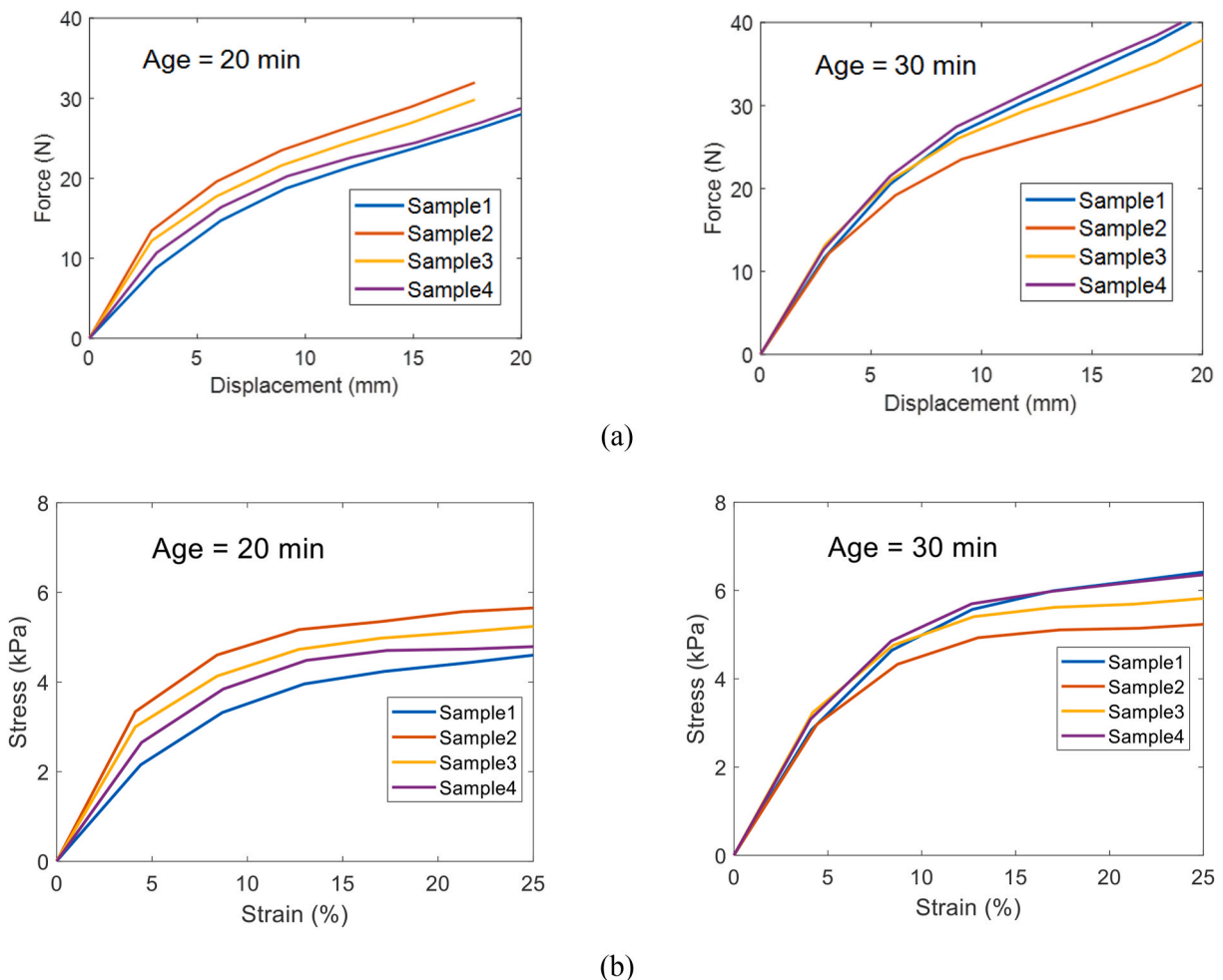

(a)

(b)

Fig. 4. Green strength test results (a) load-displacement curves (b) stress-strain curves.

performed on the cylindrical samples, which were 70 mm in height (*h*) and 70 mm in diameter (*d*), at a rate of 0.5 mm/s in an Instron equipped with a 150 N load cell with an accuracy of 0.1 N. The green strength tests are performed on casting samples. This test was performed at two fresh mortar ages of *t* = 20 and 30 min. Here, *t* = 0 was defined as the moment when the water was added to the dry mixture. The whole process, including casting, compacting, demolding and placing of samples on the test setup, takes approximately 20 min. When the time arrives at 20 min, the green strength tests were performed. The displacement is measured through the stroke of the machine. In total, 4 samples were tested for each fresh mortar age. The experimental derived load-displacement curves and computed stress-strain curves are given in Fig. 4. The failure of 3D printable material at the fresh stage is maximum stress of this curve. It can be illustrated that the material compressive strength is found to be 5.1 KPa. The sample stress under a load of 5 N is 1.3 KPa, which is less than 30% of early-age compressive strength. This stress level is thought to be outside of the non-linear creep domain, which often results in microcracks within the tested samples [38,39]. On the other hand, this load level results in the creep deformation that can be measured with a high accuracy within the machine sensitivity.

2.2.2. Creep test

2.2.2.1. Sample preparation. Early-age creep tests under uniaxial compressive loading were performed on cylindrical specimens. The sample used in the creep test is 70 mm in height and 70 mm in diameter. The PVC tube is used to make this mould. The testing samples are designed with the *h/d* ratio of 1 to minimize or eliminate the risk of structural instability during testing. The sample preparation included mixing, placement, and compaction processes, which take around 10 min in total. Subsequently, the prepared samples are placed in the mould for approximately 10 min with a sealed cover on the top. The sample for the creep test is then demolded using specialized demolding equipment (as illustrated in Fig. 5 (a)). This ensures that the sample remains upright, thereby preventing the occurrence of eccentric loading. Oil is used in the mould to reduce friction. In addition, this minimizes the water loss. The absence of bleeding during sample preparation and testing process shows that there is sufficient VMA to ensure water retention [34].

2.2.2.2. Creep testing. Here, a quasi-static compressive loading-unloading cycle test is performed to characterize the early-age creep behaviour of 3D printable material. In total, 3 samples were tested via this kind of quasi-static compressive loading-unloading cycle experiment, resulting in a total of 21 groups of creep curves. The test is based on the previous research of Irfan-ul-Hassan et al. [22]. Since it is difficult to keep the top surface of the testing specimen at fresh stage completely flat in the fresh stage, a rotation boundary condition is introduced into the specialized creep setup. For the loading to remain centric, the compressive loading is transferred from a loading point to a rotatable steel plate, which can slightly rotate. Therefore, the creep loading can be applied to the whole upper surface and with a minimum localized damage can be achieved. Meanwhile, the relative humidity (RH) and the environmental temperature were measured and remained constant during the testing process, i.e., 32% RH and 24 °C. Thus, the plastic shrinkage due to the water loss and temperature fluctuation can be significantly reduced.

This study aims to experimentally derive the creep deformation of 3D printable materials at different hardening times, which refers to clearly different microstructures due to the hydration process and consolidation settlement under a compressive load distribution. The early-age creep experimental program consists of quasi-instantaneous compressive loading-unloading cycles, as well as 180-s (3 min) holding periods in each step. Each cycle takes 10 min. Since hydration of cementitious materials is a continuous process, the microstructure cannot remain completely unaltered due to flocculation and structuration in the 180 s loading duration. The determination of loading duration for an early-age creep test must take into account microstructure change and gather sufficient data on creep evolution. For a creep test, an infinitely short loading duration would be desirable given the unchanged microstructure. Long loading durations are preferred for the creep evolution because they provide more data for creep compliance surface calibration. As a result, selecting a suitable loading duration requires taking microstructure and creep evolution into account. Here, inspired by Irfan-ul-Hassan et al. work [22] work, we adopted 180 s as the loading duration. The microstructure is assumed to be unaltered in this loading duration compared to several hours' hydration process at the fresh stage. In the remaining 7 min, a compressive force of 0.2 N ensures that the sample remains upright. The creep strain rates induced by this stable
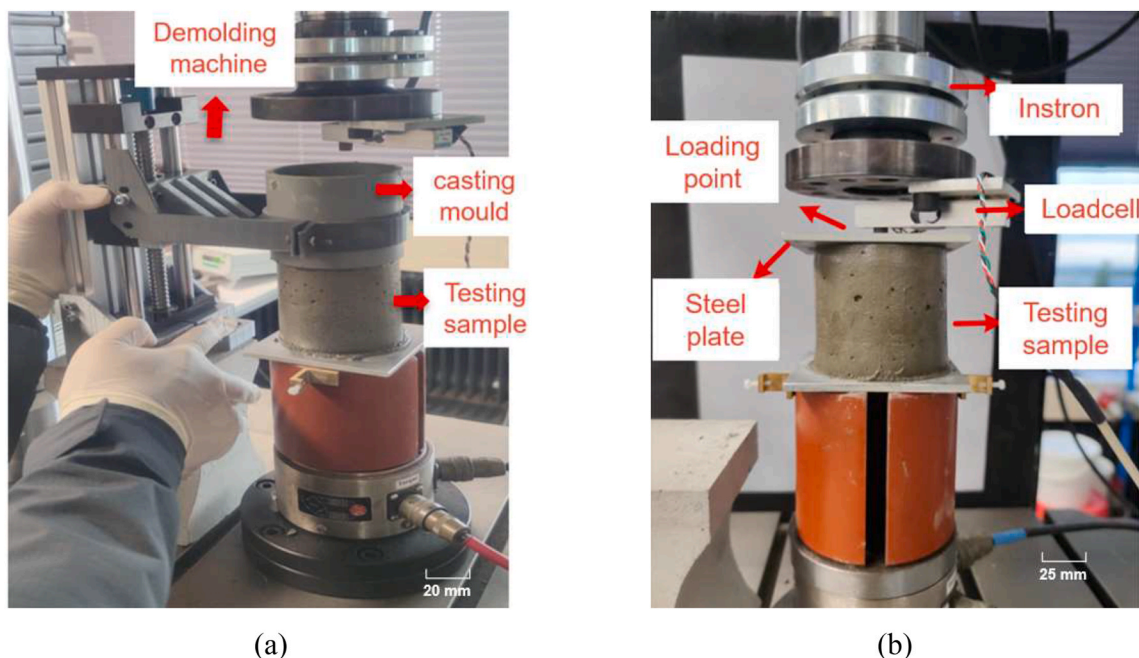

(a)   (b)

Fig. 5. Self-developed experimental setup (a) demolding setup (b) creep test setup.

load decay quickly, such that they can be neglected compared to the significantly larger creep strain captured during the 3-min testing process. The early-age creep tests were performed at multiple fresh mortar ages in the range of 20–90 min after material casting.

An infinite loading speed is desirable for a creep test, which is of course not possible. Herein, a force-controlled approach is utilized, with a prescribed loading rate of 2.5 N/s, which corresponds to a stress rate of around 1 kPa/s. The overall loading time is 2 s. This quick loading rate ensures that the loading duration is around two orders of magnitudes less than the subsequent constant loading duration of 180 s. Unloading procedure is performed via a force-controlled stress rate, amounting to 1 MPa/s Following an initial acceleration and before the piston's final deceleration, a constant creep loading is kept on the tested sample during 180 s loading duration. Fig. 6 shows the physical force path and displacement measured during this loading-unloading creep test. Structural deformation during one loading-unloading event is depicted in Fig. 7.

3. Analytical modelling

3.1. Theoretical background

The early-age creep deformation is a time-dependent process under constant loading condition. Since the creep loading in this study is below 30% of green strength, the tested sample is assumed to be in the undamaged stage. The entire loading path includes a series of loading steps, and the creep behaviour is assumed to be independent of one another under various loading steps. Therefore, the previous loading condition does not affect the creep deformation in subsequent stages. As a result, the entire creep response of the printed segments at all time steps can be computed based on the Boltzmann superposition principle, as described in Eq (1).

$$\varepsilon(t) = \int_o^t J(t-\tau,\tau)d\sigma(\tau) \qquad (1)$$

Here, J refers to the creep compliance function determined by the hardening time (τ) and loading duration (t-τ); $\Delta\sigma$ is the incremental stress, which may alter due to hydration process and loading condition. Creep occurs in hardened cementitious materials due to the slip between C–S–H particles in a shear process where water acts as lubricant [30,40]. However, the mechanism behind the early-age creep is unknown. While herein an experimental program to investigate the early age creep and analyze creep compliance using the linear viscoelastic theory is

proposed, study of governing mechanisms of this behaviour is beyond the scope of this study.

In 3DCP, each printed segment experiences increasing loading conditions due to the subsequent printing layers. The stress history of each printed segment can therefore be divided into a series of loading stages with the time interval Δt. The creep force is applied to the testing sample at the beginning of the interval, and remains constant until the end of the interval (as shown in Fig. 8 (a)). During the entire printing process, the structural deformation shows a significant development including the elastic and creep deformation. The red lines in Fig. 8 (b) represent the instantaneous elastic deformation caused by the incremental creep load at the onset of each time interval, whereas the black lines refer to the creep evolution under constant loading at this time interval.

Followed by Eq (1), the creep evolution after t_3 is the summation of all the strain curves (i.e., dashed grey curves in Fig. 7, which can be expressed as:

$$\varepsilon(t) = \sigma_1 J(t-t_0,t_0) + (\sigma_2-\sigma_1)J(t-t_1,t_1) + (\sigma_3-\sigma_2)J(t-t_2,t_2) \qquad (2)$$

It can be illustrated that a creep compliance function related to hardening and loading duration is required for structural deformation prediction. In this research, early-age creep experiments at multiple fresh mortar ages will be used to describe this relationship using an analytical model.

3.2. Quantification of creep behaviour

Fig. 6 (b) shows measured deformation of the tested sample when subjected to compressive creep loading. The initial loading-unloading step causes a comparatively significant proportional plastic deformation. One of the potential causes may be the collapse of macropores/ large air voids as a result of the compressive loading. This type of irreversible deformation is not taken into consideration in the creep analysis in order to decrease or eliminate its influence on the computation of creep compliance. When analyzing the experimental data, the second loading-unloading step is where the creep analysis begins, and the initial displacement at the onset of this loading duration is taken as the reference point for this step's creep computation.

In this work, the creep behavior at different fresh mortar ages under the constant loading is characterized using a power-law expression (as described in Eq. (3) [41].

$$\varepsilon(t-t_0,t_0) = \sigma \times C(t-t_0,t_0)$$
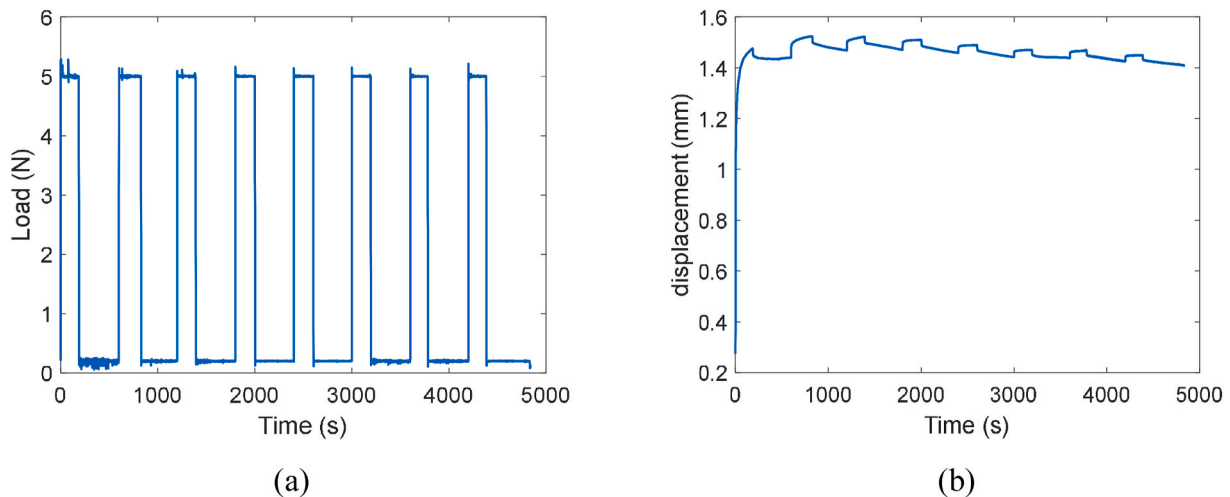$$C(t-t_0,t_0) = 1\big/E_e + 1\big/E_c \times (t-t_0)^b \qquad (3)$$

Fig. 6. Typical force reading capture during the creep test (a) loading path (b) structural deformation (Note that the time 0 in the figures refers to the mortar age of $t = 20$ min).
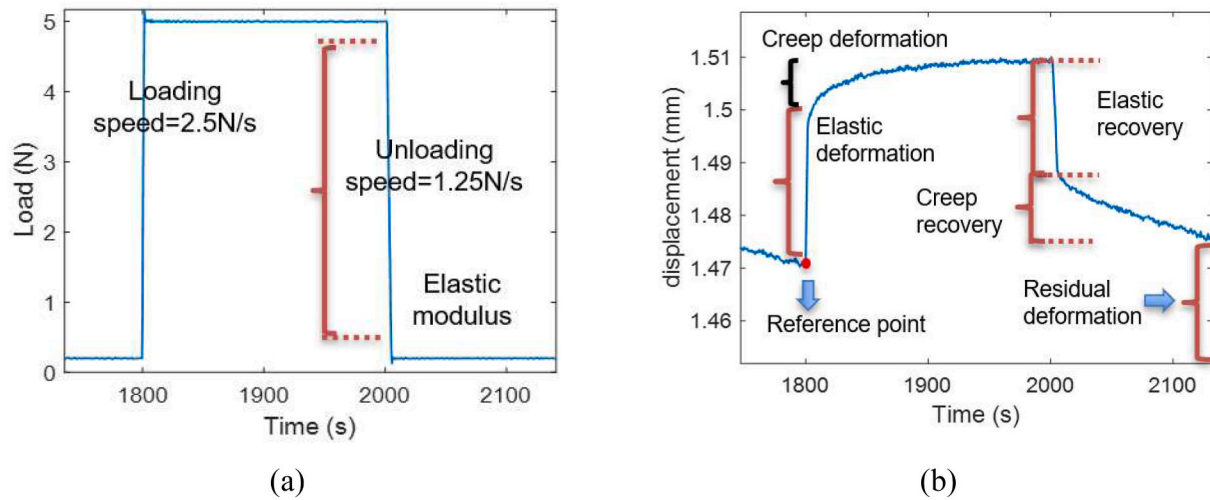
Fig. 7. Typical loading path and structural deformation in one cycle (a) loading path (b) structural deformation.
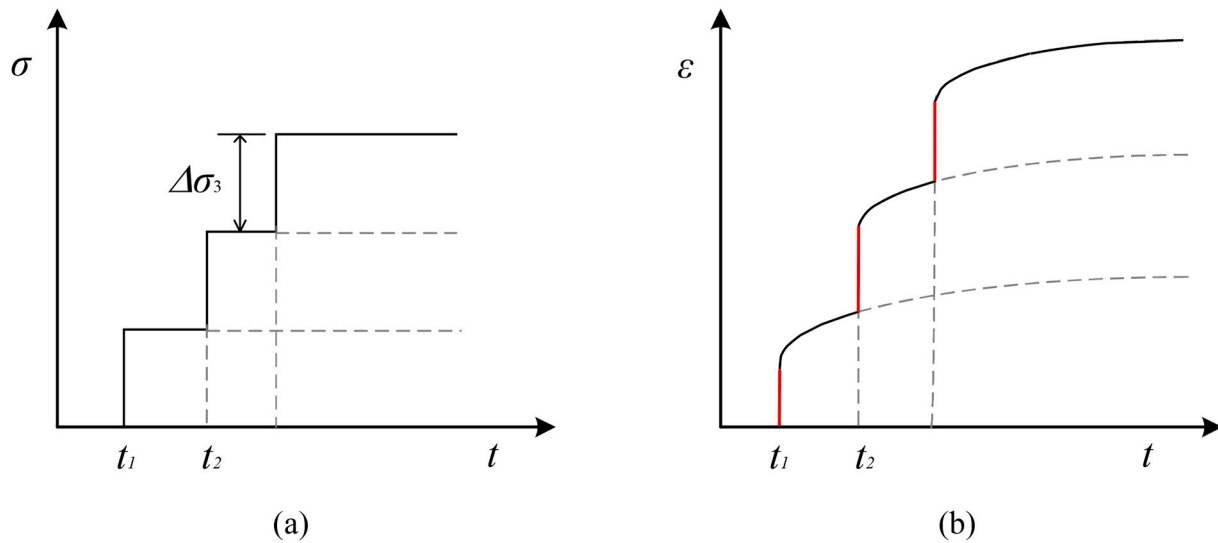

Fig. 8. Illustration of creep evolution based on superposition principle: (a) loading history (b) system deformation.

Here, E_e is the elastic modulus, E_c refers to the creep modulus and b is the creep power-law exponent. Through the evaluation of the minimal square creep strain between experimental findings and the analytical model, a set of creep coefficients, comprising creep modulus, elastic modulus, and creep exponent, can be fitted for each creep interval time [22]. In Section 4, there will be a further explanation of the fitting formulations.

The relationship between creep compliance and loading time at different hardening times can be determined using Eq. (3). The effect of hardening time on the prediction of creep compliance, however, is not well captured or reflected by the fitted power-law function. A double power law expression based on the two international standard codes Euro Code 2 [31] and ACI-209R [32] offers a solution to this problem, and their formulation can be uniformly described as:

$$J(t-\tau,\tau) = 1 / E(\tau) + C_0 C_1(\tau) C_2(t-\tau) \qquad (4)$$

Here, C_0 is a coefficient related to general material properties and microstructure formation as a result of hydration, which is also affected by external conditions like temperature and relative humidity; C_1 is a power function used to study the impact of hardening time (τ) on creep compliance; and C_2 is a power function that is only determined by the

non-ageing/loading duration (t-τ) [42].

3.3. Determination of unloading elastic modulus

The unloading procedure in this quasi-static compressive creep test is utilized to determine the unloading elastic modulus [41]. Fig. 7 (a) illustrates the unloading part, where the top 10% and bottom 5% of elastic recovery occurred during the unloading process are cut away, and the left elastic recovery is utilized to compute the unloading elastic modulus. Through dividing the residual force reading by the cross-section area of the cylindrical specimen, which is equal to 3846.5 mm^2, it is possible to calculate the imposed stress. The structural strains can be computed through dividing the machine output displacement by the sample height, which is 70 mm. As a result, the unloading elastic modulus can be determined.

4. Results

The proposed early-age creep test provides quantification of temporal evolution of unloading elastic modulus and creep of 3D printable mortar in the time range of 30–90 min with a 10-min interval. Three samples are used for the test and all three exhibit similar properties. This

highlights the reliability of the testing procedures and the importance of the experimental finding will be discussed later.

4.1. Unloading elastic modulus

Fig. 7 (b) shows the elastic recovery during the unloading process, indicating that this printable material is in viscous-elastic-plastic state. As described in Section 3.2, the unloading elastic modulus can be determined through the calculation of elastic recovery through each cycle's unloading process. Fig. 9 illustrates how the time-dependent unload elastic modulus grows monotonically with material age. A linear fit can be found, as shown in Fig. 9. It should be noted that the R-square value is computed between the regression and average experimental data.

4.2. Creep compliance curves

As previously mentioned, the power-law function is adopted to fit the early-age creep behaviour in the time range from 30 to 90 min after material deposition. When calibrating the analytical model, the objective function is determined by the R-square value, which reflects the difference between the mean experimental data from three testing specimens and the power-law regression. Fig. 10 shows the temporal evolution of the creep modulus and calibrated power-law functions at various material ages.

It can be seen in Fig. 10 that the power-law function can fit the early-age creep behaviour with high R^2. Fig. 9 describes the development of time-dependent creep parameters with hardening time. Both the creep modulus and elastic modulus increases with the hardening time. Note that this type of delayed deformation differs from the basic creep in hardened cementitious materials. As previously discussed, it is determined by the combined effect of hydration process and consolidation settling under compressive stress distribution. However, this experimental program makes it possible to mimic the time-dependent deformation that occurs in printing trials, which is what we want to measure.

Based on the experimentally derived creep deformation, analytical modelling was used to compute the creep compliance at different ages. However, the creep deformation during the printing process is associated with mortar age and loading duration, thus a clear relationship between creep compliance and hardening time and loading duration is required.
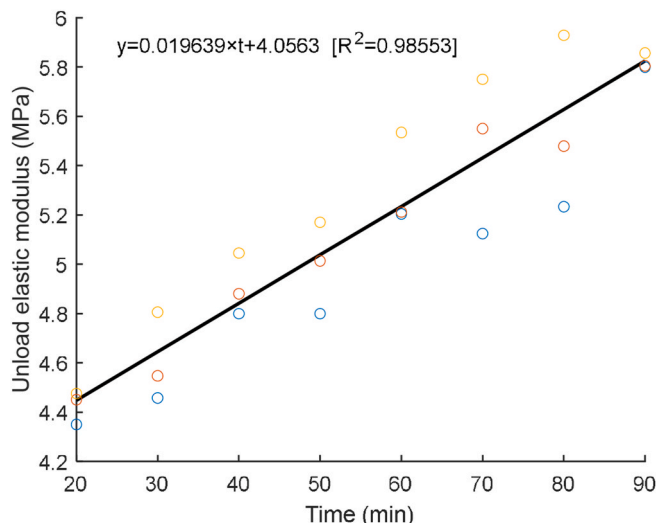
4.3. Creep compliance surface

The influence of hardening time and loading duration on creep deformation can be reflected in a creep compliance surface, as discussed in Section 3.2. Here, a double law power expression in Eq. (4) is used to describe this relationship. The smallest square root (i.e., the difference between the fitted function surface and experimental data) can be obtained using the optimal creep parameters, which are composed of C_1, C_2, C_3 and E. Fig. 12 describes the fitted creep compliance surface after optimization process.

4.4. Evolution of early-age material properties with hardening time

In this study, this specialized experimental program consists of a 180 s loading period, in which the microstructure almost remains unaltered due to flocculation and structuration. It should be noted that hydration process of cementitious materials is a continuous process, the microstructure is impossible to absolutely remain unaltered due to flocculation and structuration in the 180 s loading duration. The microstructure change within 180 s is assumed to be small compared to the first several hours' hydration process. The experimental results at multiple material ages refer to the different stages of the hydration process. The evolution of unloading elastic modulus and creep modulus describes the impact of hydration process on the material properties. In 3DCP, the printable materials are extruded from the nozzle and placed on the printed structure. The hydration process continues throughout this stage resulting in varying microstructures. From a microstructural perspective, the flocculation and structuration processes make the printed materials display the initial material characteristic such as yield stress and elastic behaviour. The mixing and pumping processes disperse the cement particles throughout the printing process. After flocculation, these particles connect to form a network that can transfer stress. The elastic material behaviour results from attractive colloidal force while the viscous property is primarily caused by the interstitial water between the cement grains. Although the printable mortar is still in the rest state, solid bridges between the interconnected particles are formed when hydrate nucleation occurs at pseudo-contact points in the network of particles. The structuration process strengthens the bonding among inter-particle connections and causes the loss of workability [43]. Additionally, it can be seen that a stronger framework eventually develops at the microscopic level along with the hydration process. As a result, the elastic modulus increases at the macroscopic level with hydration time, so does creep modulus.

Besides the hydration process, the consolidation settlement under compressive loading another factor for the measured early-age creep in this study. A lot of free space exists between the dispersed cement particles. These dispersed particles are gradually compacted and eventually collapse when subjected to compressive force. This compaction process is similar to the consolidation settlement in soil mechanics [44,45]. If more voids are compressed, less deformation space may indeed be found. The entire structure has a higher material density as a result. Therefore, on the macroscale, both the elastic modulus and creep modulus increase with hardening time.

5. Model validation

The fitted creep compliance surface allows predicting creep deformation with the loading condition and printing time as inputs. To verify if this analytical model can predict the early-age creep deformation during printing process, an incremental loading test is designed to mimic the loading condition in 3DCP. The cylindrical sample is the same size as in the previous creep test. In total, 4 samples were tested for model validation. Fig. 13 describes the loading path and obtained structural deformation. The first loading step results in a significant plastic deformation, like the early-age creep test. When analyzing the structural deformation, the onset point of the second loading step is taken as the
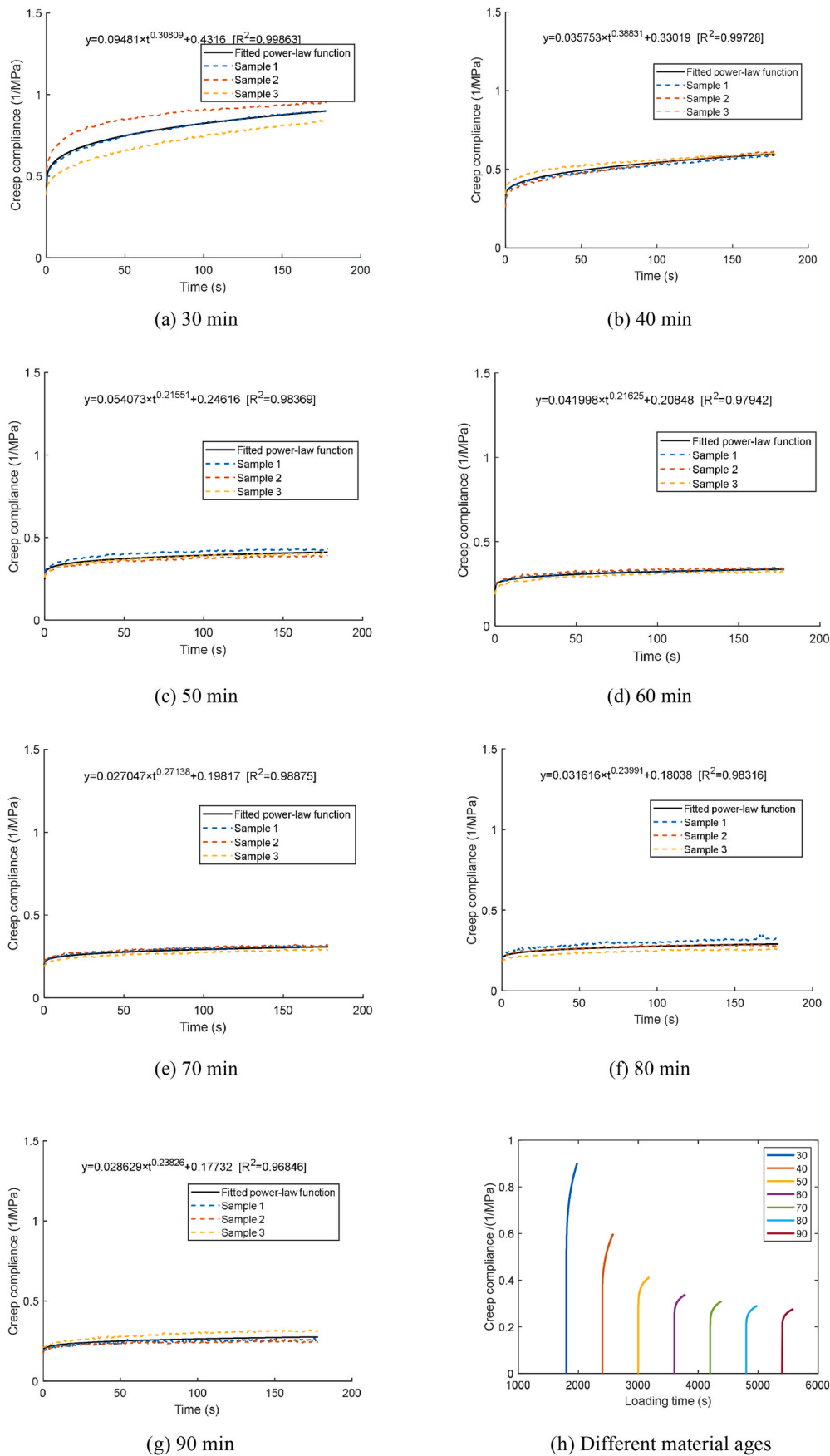
Fig. 9. Time-dependent unloading elastic modulus.

Fig. 10. Time-dependent creep compliance at different aging time.
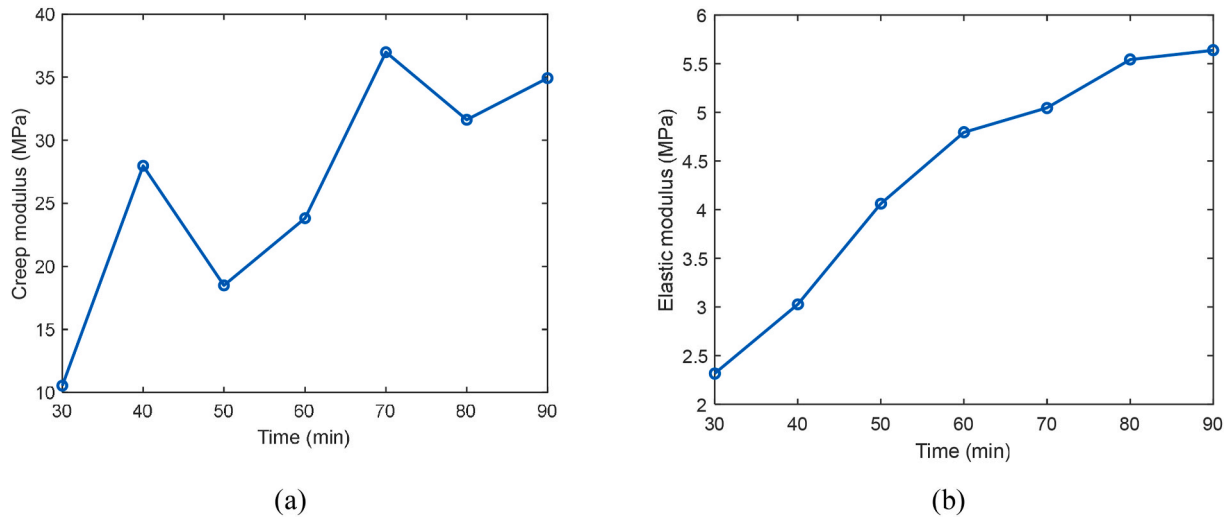
Fig. 11. Evolution of creep parameters with the increasing age of printable material (a) creep modulus with hardening time (b) elastic modulus with hardening time.
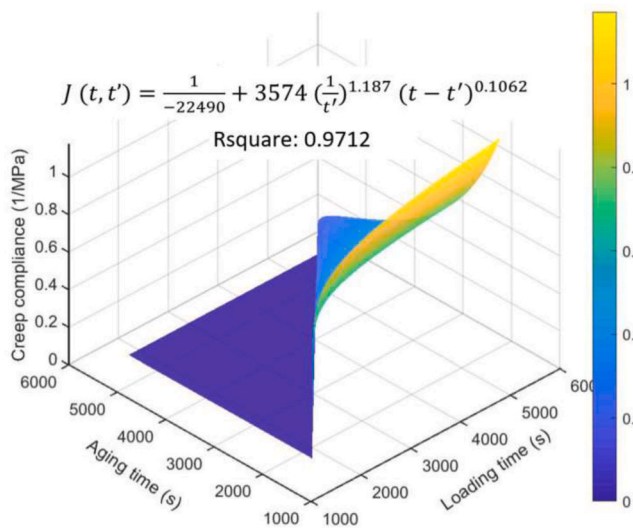

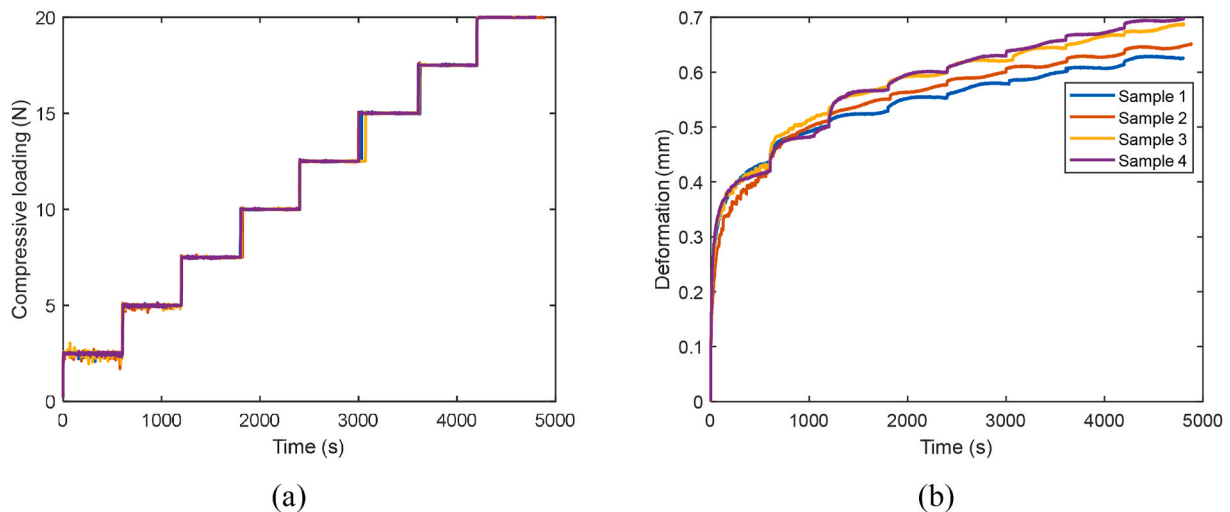**Fig. 12.** Calibrated creep compliance surface.

moment at which data analysis begins.

For creep prediction, the entire loading process can be divided into a series of loading sequences, each assumed to remain constant from the onset of time interval to the end. As a result, the material behaviour of early-age creep under various loading conditions is independent of one another. This means that the creep deformation that occurred at later stages is unaffected by the previous loading condition. Thus, the entire creep response of this sample at all time steps can be computed based on the Boltzmann superposition, as described in Section 3.1. The total deformation of the sample is a summation consisting of elastic and creep portions.

Fig. 14 demonstrates that analytical modelling of the early-age creep can quantitatively reproduce the experimental results. This indicates that the analytical modelling can account for the stress history and reproduce the time-dependent deformation during the printing process. However, there is still some discrepancy between the analytical solution and the experimental data, especially in the initial phase. The variability of the creep data from compressive test could be one of the causes. In particular, the creep loading lower than 30% of compressive strength is used to determine the early-age creep behaviour. This is because that stress level is within the linear creep domain, which excludes the impact of damage on the time-dependent deformation. However, as discussed
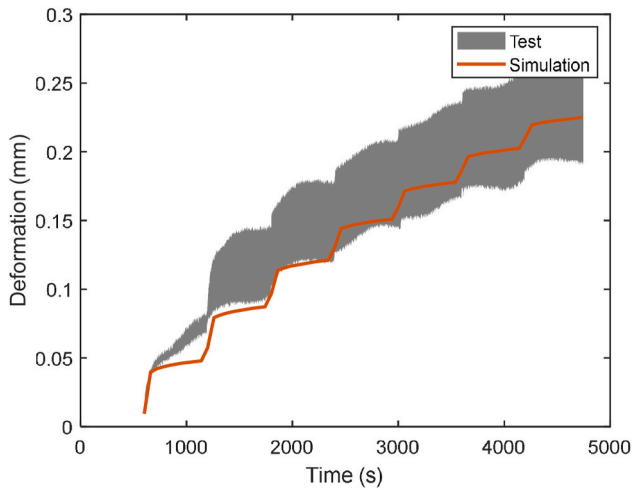

Fig. 13. Compressive creep test with incremental loading (a) loading path (b) structural deformation (Note that the time 0 in the figures refers to the mortar age of t = 20 min).

Fig. 14. The comparison results between the analytical solution and experimental result (Note that the time 0 in the figures refers to the mortar age of t = 20 min).

before, this assumption origins from creep analysis of hardened cementitious materials. The validity of this assumption may be challenged for cementitious materials at the fresh stage, in which the creep mechanism is unclear and at possibly different. In the following section,

more creep tests with various loading magnitudes are conducted to study the impact of load level on the creep compliance.

6. Discussion

6.1. The impact of load level on creep compliance curves

Herein, the same experimental program but with different compressive loading (i.e., 2.5 N and 10 N) is used to characterize the early-age creep behaviour at the multiple mortar ages: t = 30, 40, 50, and 60 min. Figs. 15 and 16 show the experimental findings as well as the calibrated creep curves based on the power-law function. R square reflects the difference between the mean experimental data from three testing specimens and the power-law regression. The fitted results demonstrate that the power-law expression is able to represent the evolution of early-age creep under different magnitudes of compressive loading. Fig. 17 describes the evolution of elastic modulus and creep modulus with hardening time at different loading conditions. The experimental finding verifies the previous conclusion, i.e., both the elastic and creep modulus increase with the hardening time. In addition to the relationship depicted in Fig. 11, all of them reveal the same tendency between creep parameters, consisting of elastic modulus and creep modulus, and mortar age.
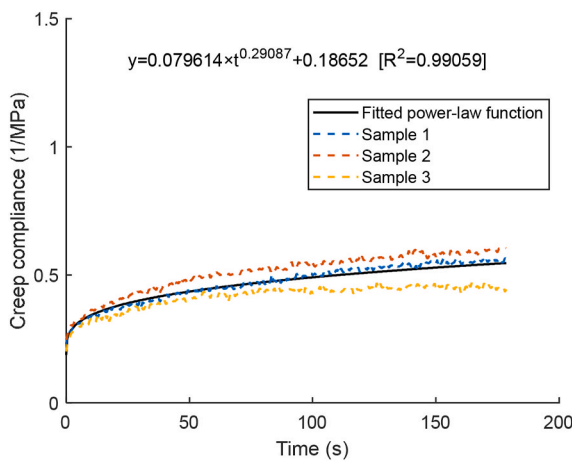
Fig. 18 shows a comparison of creep compliance with different loading magnitudes for sample ages from 30 to 60 min. It is found that the creep compliance decreases as the loading increases. This can help to
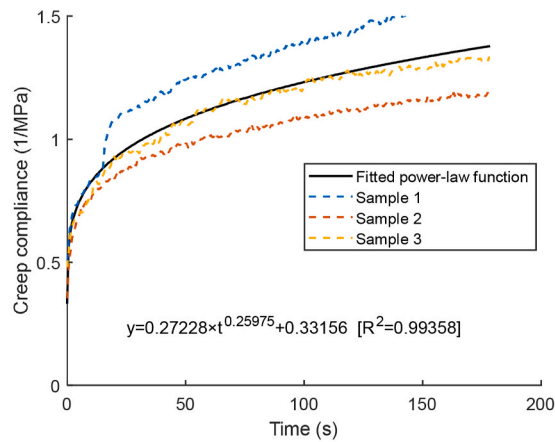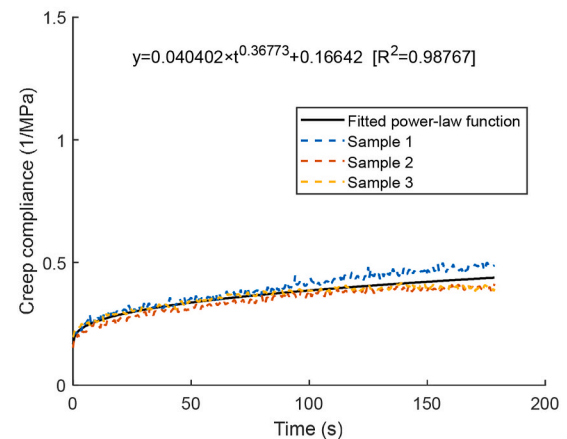

(a) 30 min
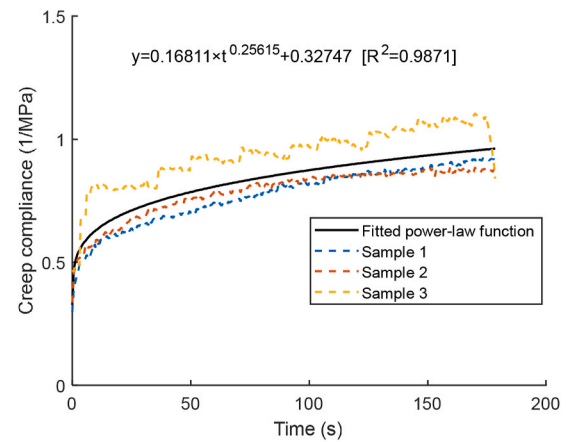
(b) 40 min

(c) 50 min

(d) 60 min

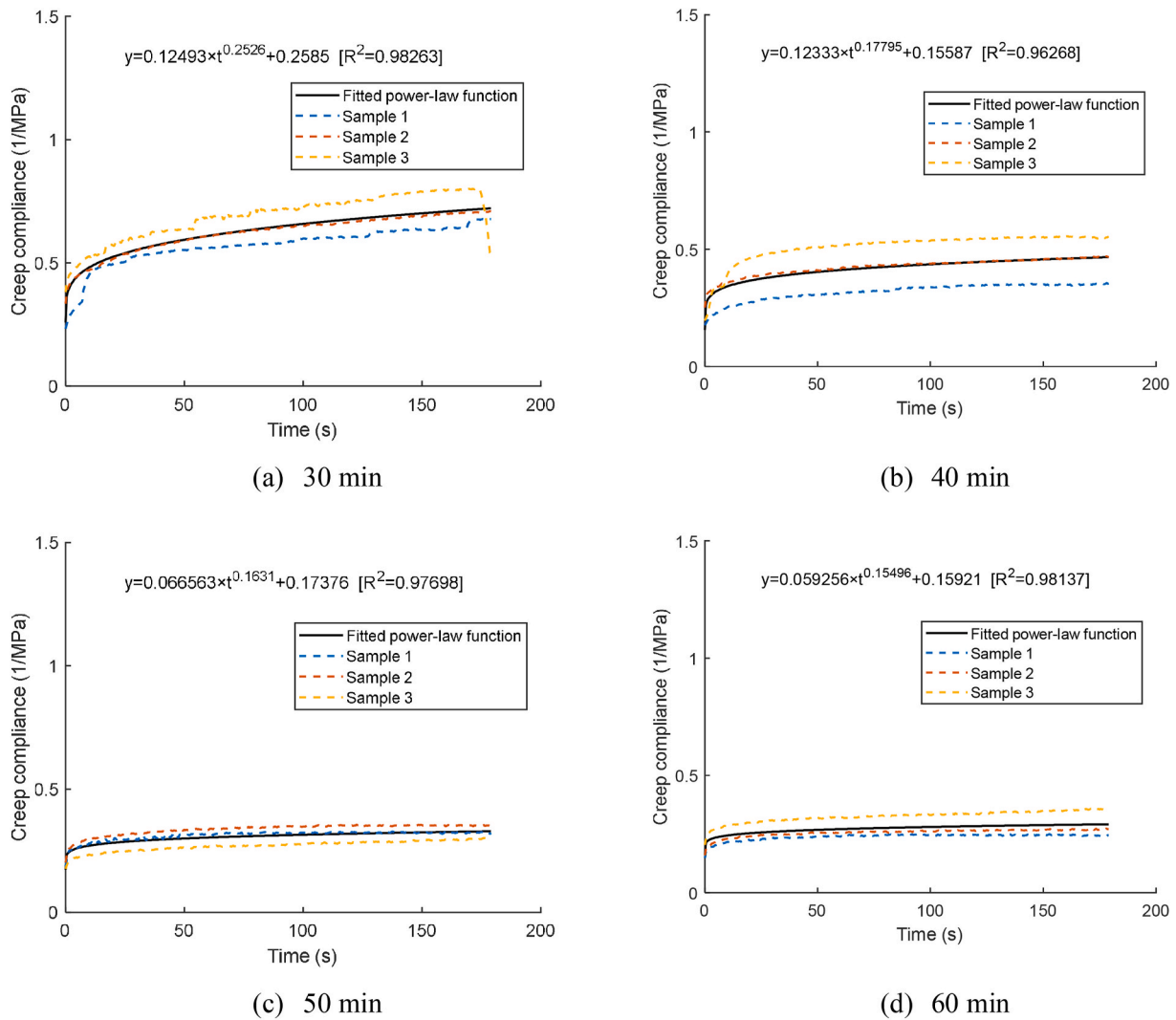**Fig. 15.** Creep compliance curves with the compressive load of 2.5 N.

Fig. 16. Creep compliance curves with the compressive loading of 10 N.

explain a slight discrepancy between the experimental results and analytical prediction, most notably at the beginning of the test. It is possible that the creep compliance for 3D printable mortar in the fresh stage depends on the load level. More specifically, experimental results from the creep test under 5 N are used to determine the creep compliance. However, the validation test adopts incremental compressive loading starting at 2.5 N with a 2.5 N increment. At the beginning of the test, the compressive load applied to the sample is below 5 N. However, the creep compliance surface obtained from 5 N is adopted to predict the creep deformation. A small difference between the testing results and analytical prediction therefore can be observed.

The reason is unclear. To the best of the authors knowledge, only one published article focused on the impact of loading magnitude on the creep compliance [31]. Experimental results from Ref. [17], shown in Fig. 19, conflict with the trends observed herein. In that work, a very small shear force is applied to 3D-printed calcium sufflaminate cement composites using a rheometer to characterize the early-age creep. Their experiments show that the creep compliance increases with the applied shear stress. The rheological test measures the bonding force among particles, which is attributed to the impact of flocculation and structuration. In the rheological test, a higher shear stress can create more microcracks, therefore, creep increases with the stress level. In contrast, the uniaxial compression test measures the creep evolution with the consideration of the compaction process and pore effect. The creep feature is somewhat similar to the time-dependent deformation of 3D

printed segments with high porosity [29,46]. During the test, the impact of pores or air voids will be reflected through the creep behaviour in macroscale. The higher compressive stress compacts more pores within the tested sample. With the increased compressive load, there are less voids within the tested sample which can be compressed, thereby resulting in less creep. Compared to the rheological test, this kind of uniaxial compression test mainly reflects the impact of compressed internal voids within the tested sample on creep evolution.

6.2. Volumetric strain under incremental compressive loading

To further verify the above hypothesis, a specialized experimental program is designed to characterize the volumetric strain under the compressive force. Fig. 20 describes the experimental setup. Two samples are used to test the repeatability of the testing protocol. During the testing process, a camera is utilized to capture sample deformation, and an incremental vertical compressive load is applied at the rate of 0.01 mm/s. The volume of the tested sample in each step is computed based on the horizontal and vertical deformation, as shown in Fig. 20.

Fig. 21 (a) describes the normalized volumetric strain, which is defined as the ratio between the loaded sample volume and the initial one, versus structural vertical strain. It can be observed that the lowest normalized volumetric strain occurs at structural strain about 1%. This suggests that the free space, consisting of pores or voids between cement particles, is compacted under the compressive loading until that vertical
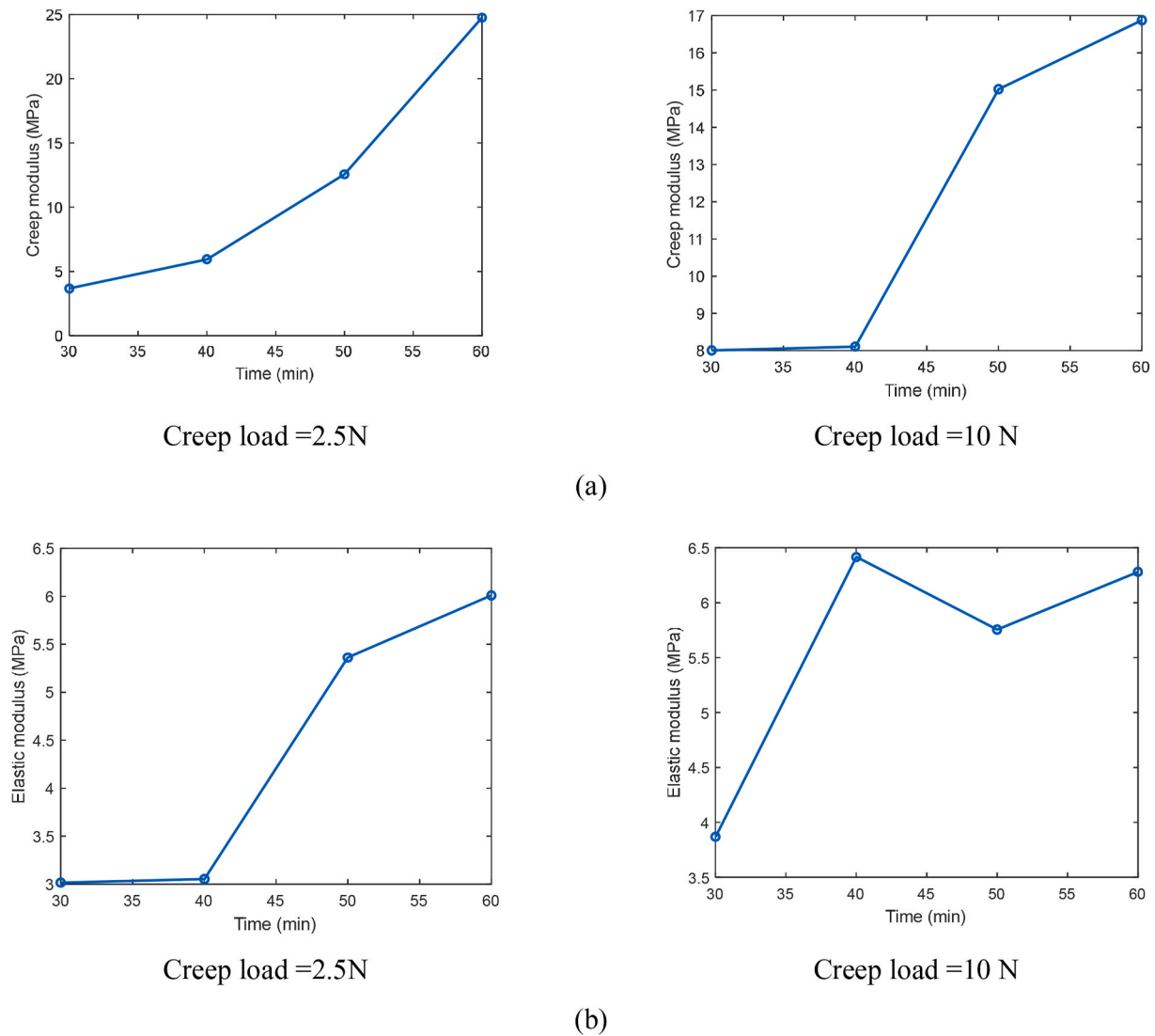
Creep load =2.5N

Creep load =10 N

(a)

Creep load =2.5N

Creep load =10 N

(b)

Fig. 17. The relationship between the creep parameters and hardening time (a) creep modulus (b) elastic modulus.

stain reaches 1%. After that, a transition of the measured curves can be found, and expansion is observed due to the Poisson's effect. It suggests that the testing sample is more difficult to compress when it exceeds 1% strain. Fig. 21 (b) gives a relationship between compressive loading with structural vertical strain. It can be easily found the equivalent compressive loading at 1% sample strain is below 5 N. According to this inflexion point, the samples are easily compressed up to a structural vertical strain of 1%, whereas after that point, specimens with collapsed large pores are difficult to compress under a unit compressive loading. As a result, the largest creep compliance obtained from a compressive creep test with 2.5 N creep loading can be derived.

7. Conclusions

In this study, an experimental setup was proposed to characterize the early-age elastic and creep behaviours of 3D printable mortar. The experimental program consists of quasi-static compressive loading-unloading cycles as well as 180-s holding periods in between. Based on the experimental results, a double power-law model can be used to predict the creep compliance with the inputs of hardening time and loading duration. Subsequently, this analytical model was validated by comparison to uniaxial compression tests with incremental loading. Based on this research, the following conclusions can be drawn.

(1) The printable mortar at fresh stage is visco-elastic plastic; the elastic recovery can be observed during the unloading process and the unloading elastic modulus also can be derived;

(2) The power-law expression can describe the early-age creep behaviour; both the elastic modulus and the creep modulus increase with hydration time; the possible reasons include consolidation settlement under compressive loading and the hydration process, consisting of flocculation and structuration;

(3) This quasi-static compressive creep test characterizes the early-age creep behaviours at multiple mortar ages. The experimental results are based on a double law power expression to describe the creep compliance with the hardening time and loading duration;

(4) Analytical modelling of early-age creep behaviour during printing process reproduces the experimental results quantitatively; it demonstrates the feasibility of proposed method for time-dependent structural deformation prediction in 3DCP; A small discrepancy between the analytical solution and the experimental data can be found, especially in the initial phase. This is because the underestimation of creep compliance due to the magnitude of creep loading;

(5) The higher compressive stress indeed results in a lower creep compliance. The inverse tendency can be found from the
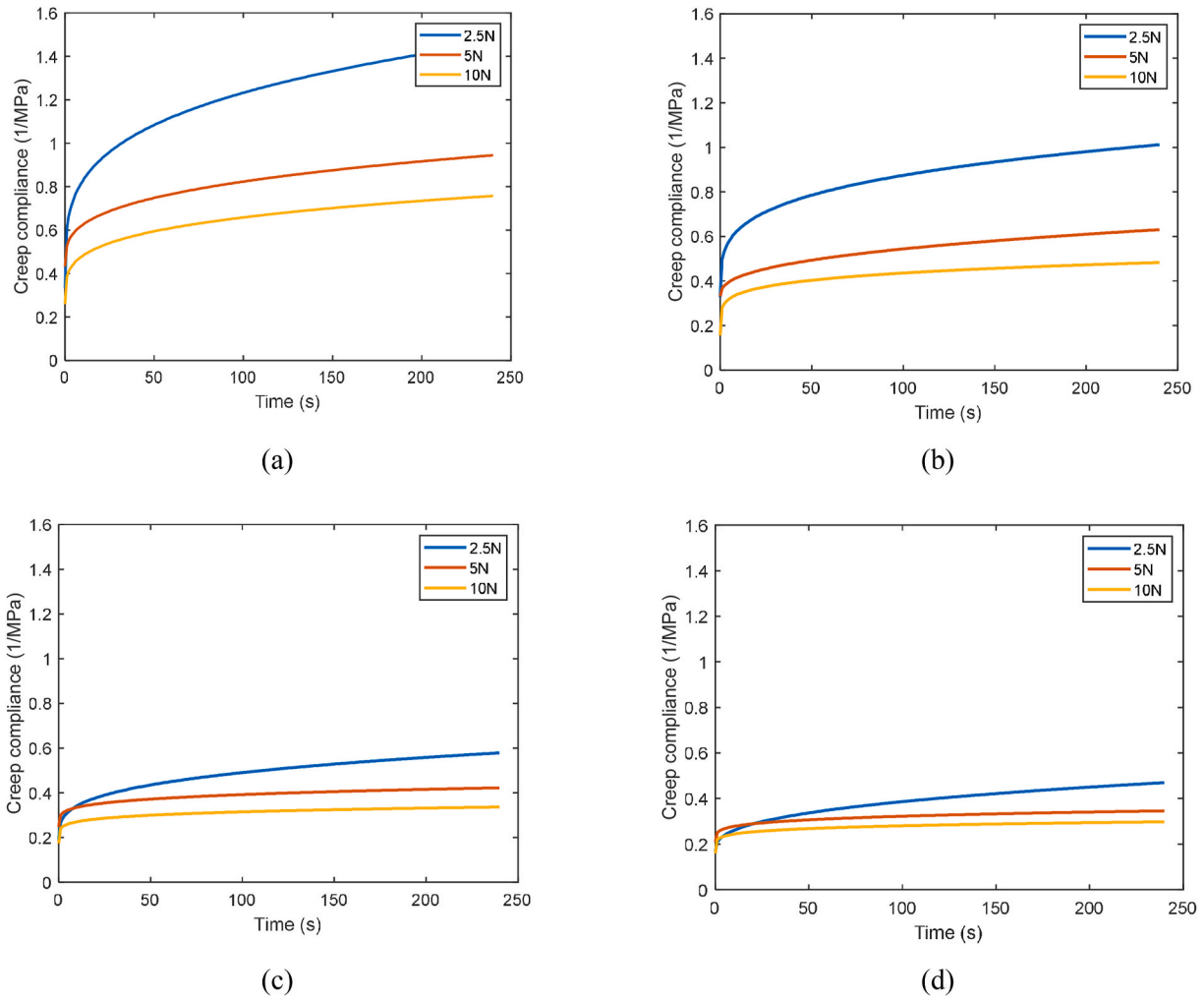
Fig. 18. The creep compliance curves with different compressive loading (a) 30min (b) 40 min (c) 50 min (d) 60 min.
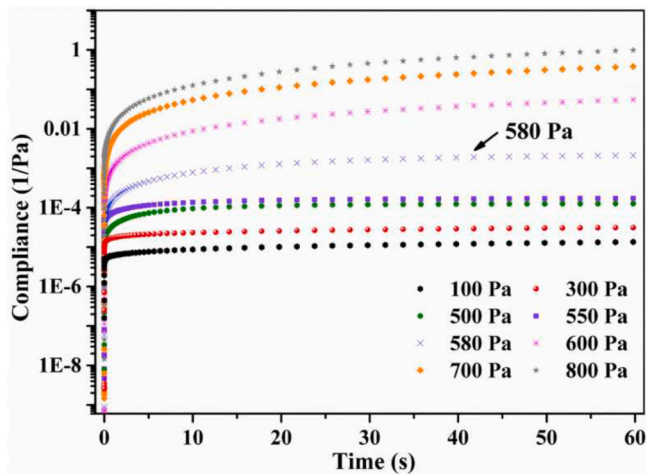

Fig. 19. Typical creep curves of cementitious materials obtained using rheometer using various shear stress, reproduced from Ref. [31].

Fig. 20. Experimental setup for volumetric strain capture.

rheological test in the literature. This is because the different measured characteristics towards these two methods. In the rheological test, a higher shear stress can create more micro-cracks, therefore, creep increases with the stress level. In contrast,
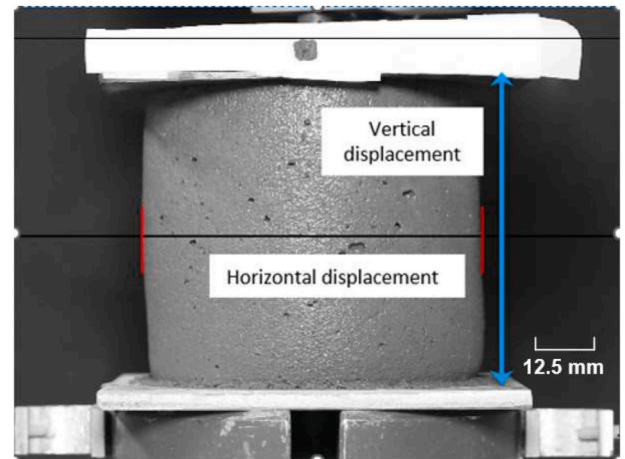
this uniaxial compression test mainly reflects the impact of compaction process and internal pore on creep evolution.

Through this study, the time-dependent deformation during the printing process in 3DCP can be precisely predicted through a combination of analytical modelling and experimental investigation. Further
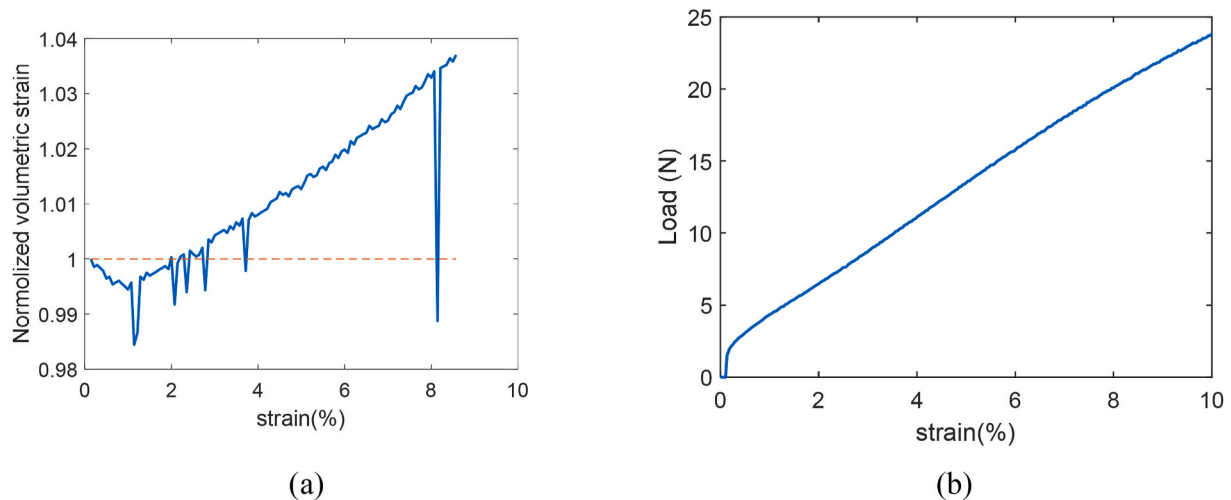
Fig. 21. Volumetric strain between the experimental program (a) volumetric strain versus sample strain (b) applied force with sample strain.

research will be conducted to study the impact of early-age creep evolution on the prediction of structural deformation and buildability quantification during the printing process of 3DCP.

Declaration of competing interest

The authors declare that they have no known competing financial interests or personal relationships that could have appeared to influence the work reported in this paper.

Data availability

Data will be made available on request.

Acknowledgements

References

[1] R.A. Buswell, W.R. L d S., S.Z. J, D. J, 3D printing using concrete extrusion: a roadmap for research, Cement Concr. Res. 112 (2018) 37–49.

[2] F. Bos, R. Wolfs, Z. Ahmed, T. Salet, Additive manufacturing of concrete in construction: potentials and challenges of 3D concrete printing, Virtual Phys. Prototyp. 11 (3) (2016) 209–225.

[3] V. Mechtcherine, F.P. Bos, A. Perrot, W.L. da Silva, V. Nerella, S. Fataei, R.J. Wolfs, M. Sonebi, N. Roussel, Extrusion-based additive manufacturing with cement-based materials–Production steps, processes, and their underlying physics: a review, Cement Concr. Res. 132 (2020), 106037.

[4] D. Asprone, F. Auricchio, C. Menna, V. Mercuri, 3D printing of reinforced concrete elements: technology and design approach, Construct. Build. Mater. 165 (2018) 218–231.

[5] R. Jayathilakage, P. Rajeev, J. Sanjayan, Extrusion rheometer for 3D concrete printing, Cement Concr. Compos. 121 (2021), 104075.

[6] A. Perrot, A. Pierre, V. Nerella, R. Wolfs, E. Keita, S. Nair, N. Neithalath, N. Roussel, Mechtcherine, from analytical methods to numerical simulations: a process engineering toolbox for 3D concrete printing, Cement Concr. Compos. 122 (2021), 104164.

[7] C. Gosselin, R. Duballet, P. Roux, N. Gaudillière, J. Dirrenberger, P. Morel, Large-scale 3D printing of ultra-high performance concrete – a new processing route for architects and builders, Mater. Des. 100 (2016) 102–109.

[8] T.A. Salet, Z.Y. Ahmed, F.P. Bos, H.L. Laagland, Design of a 3D printed concrete bridge by testing, Virtual Phys. Prototyp. 13 (3) (2018) 222–236.

[9] R. Naboni, L. Breseghello, A. Kunic, Multi-scale design and fabrication of the trabeculae pavilion, Addit. Manuf. 27 (2019) 305–317.

[10] J. Kruger, S. Zeranka, G. van Zijl, 3D concrete printing: a lower bound analytical model for buildability performance quantification, Autom. ConStruct. 106 (2019), 102904.

[11] V.N. Nerella, M. Krause, V. Mechtcherine, Direct printing test for buildability of 3D-printable concrete considering economic viability, Autom. ConStruct. 109 (2020), 102986.

[12] Z. Chang, Y. Xu, Y. Chen, Y. Gan, E. Schlangen, B. Šavija, A discrete lattice model for assessment of buildability performance of 3D-printed concrete, Comput. Aided Civ. Infrastruct. Eng. 36 (5) (2021) 638–655.

[13] B. Panda, N. Mohamed, N. Ahamed, S.C. Paul, G. Bhagath Singh, M.J. Tan, B. Šavija, The effect of material fresh properties and process parameters on buildability and interlayer adhesion of 3D printed concrete, Materials 12 (13) (2019) 2149.

[14] N.W. Tschoegl, Energy storage and dissipation in a linear viscoelastic material, The Phenomenological Theory of Linear Viscoelastic Behavior (1989) 443–488. Springer.

[15] R. Wolfs, F. Bos, T. Salet, Early age mechanical behaviour of 3D printed concrete: numerical modelling and experimental testing, Cement Concr. Res. 106 (2018) 103–116.

[16] S.C. Paul, Y.W.D. Tay, B. Panda, M.J. Tan, Fresh and hardened properties of 3D printable cementitious materials for building and construction, Arch. Civ. Mech. Eng. 18 (1) (2018) 311–319.

[17] B. Panda, J.H. Lim, M.J. Tan, Mechanical properties and deformation behaviour of early age concrete in the context of digital construction, Compos. B Eng. 165 (2019) 563–571.

[18] R. Wolfs, F. Bos, T.J.C. Salet, Triaxial compression testing on early age concrete for numerical analysis of 3D concrete printing, Cement Concr. Compos. 104 (2019), 103344.

[19] N. Roussel, Correlation between yield stress and slump: comparison between numerical simulations and concrete rheometers results, Mater. Struct. 39 (4) (2006) 501.

[20] F.P. Bos, P. Kruger, S.S. Lucas, G. van Zijl, Juxtaposing fresh material characterisation methods for buildability assessment of 3D printable cementitious mortars, Cement Concr. Compos. 120 (2021), 104024.

[21] M. Briffaut, F. Benboudjema, J.-M. Torrenti, G. Nahas, Concrete early age basic creep: experiments and test of rheological modelling approaches, Construct. Build. Mater. 36 (2012) 373–380.

[22] M. Irfan-ul-Hassan, B. Pichler, R. Reihsner, C. Hellmich, Elastic and creep properties of young cement paste, as determined from hourly repeated minute-long quasi-static tests, Cement Concr. Res. 82 (2016) 36–49.

[23] L. Esposito, L. Casagrande, C. Menna, D. Asprone, F. Auricchio, Early-age creep behaviour of 3D printable mortars: experimental characterisation and analytical modelling, Mater. Struct. 54 (6) (2021) 1–16.

[24] Y. Qian, S. Kawashima, Use of creep recovery protocol to measure static yield stress and structural rebuilding of fresh cement pastes, Cement Concr. Res. 90 (2016) 73–79.

[25] Z. Sun, T. Voigt, S.P. Shah, Rheometric and ultrasonic investigations of viscoelastic properties of fresh Portland cement pastes, Cement Concr. Res. 36 (2) (2006) 278–287.

[26] S.A. Nair, S. Panda, M. Santhanam, G. Sant, N. Neithalath, A critical examination of the influence of material characteristics and extruder geometry on 3D printing of cementitious binders, Cement Concr. Compos. 112 (2020), 103671.

[27] B. Lu, Y. Weng, M. Li, Y. Qian, K.F. Leong, M.J. Tan, S. Qian, A systematical review of 3D printable cementitious materials, Construct. Build. Mater. 207 (2019) 477–490.

[28] M.K. Mohan, A. Rahul, K. Van Tittelboom, G. De Schutter, Rheological and pumping behaviour of 3D printable cementitious materials with varying aggregate content, Cement Concr. Res. 139 (2021), 106258.

[29] Y. Chen, Z. Chang, S. He, O. Çopuroğlu, B. Šavija, E. Schlangen, Effect of curing methods during a long time gap between two printing sessions on the interlayer bonding of 3D printed cementitious materials, Construct. Build. Mater. 332 (2022), 127394.

[30] B.T. Tamtsia, J.J. Beaudoin, Basic creep of hardened cement paste A re-examination of the role of water, Cement Concr. Res. 30 (9) (2000) 1465–1475.

[31] M. Chen, B. Liu, L. Li, L. Cao, Y. Huang, S. Wang, P. Zhao, L. Lu, X. Cheng, Rheological parameters, thixotropy and creep of 3D-printed calcium sulfoaluminate cement composites modified by bentonite, Compos. B Eng. 186 (2020), 107821.

[32] F.P. Bos, Z.Y. Ahmed, E.R. Jutinov, T.A.M. Salet, Experimental exploration of metal cable as reinforcement in 3D printed concrete, Materials 10 (11) (2017).

[33] Y. Chen, S.C. Figueiredo, Z. Li, Z. Chang, K. Jansen, O. Çopuroğlu, E. Schlangen, Improving printability of limestone-calcined clay-based cementitious materials by using viscosity-modifying admixture, Cement Concr. Res. 132 (2020), 106040.

[34] M. Lachemi, K. Hossain, V. Lambros, P.-C. Nkinamubanzi, N. Bouzoubaa, Performance of new viscosity modifying admixtures in enhancing the rheological properties of cement paste, Cement Concr. Res. 34 (2) (2004) 185–193.

[35] T.T. Le, S.A. Austin, S. Lim, R.A. Buswell, A.G. Gibb, T. Thorpe, Mix design and fresh properties for high-performance printing concrete, Mater. Struct. 45 (8) (2012) 1221–1232.

[36] R. Vrijdaghs, M. di Prisco, L. Vandewalle, Uniaxial tensile creep of a cracked polypropylene fiber reinforced concrete, Mater. Struct. 51 (1) (2018) 1–12.

[37] N. Ranaivomanana, S. Multon, A. Turatsinze, Tensile, compressive and flexural basic creep of concrete at different stress levels, Cement Concr. Res. 52 (2013) 1–10.

[38] M.F. Ruiz, A. Muttoni, P.G. Gambarova, Relationship between nonlinear creep and cracking of concrete under uniaxial compression, J. Adv. Concr. Technol. 5 (3) (2007) 383–393.

[39] P. Rossi, J.-L. Tailhan, F. Le Maou, L. Gaillet, E. Martin, Basic creep behavior of concretes investigation of the physical mechanisms by using acoustic emission, Cement Concr. Res. 42 (1) (2012) 61–73.

[40] H. Ye, Creep mechanisms of calcium–silicate–hydrate: an overview of recent advances and challenges, International Journal of Concrete Structures Materials 9 (4) (2015) 453–462.

[41] P. Karte, M. Hlobil, R. Reihsner, W. Dörner, O. Lahayne, J. Eberhardsteiner, B. Pichler, Unloading-based stiffness characterisation of cement pastes during the second, third and fourth day after production, Strain 51 (2) (2015) 156–169.

[42] C. Européen, Eurocode 2: Design of Concrete Structures—Part 1-1: General Rules and Rules for Buildings, British Standard Institution, London, 2004.

[43] N. Roussel, Rheological requirements for printable concretes, Cement Concr. Res. 112 (2018) 76–85.

[44] W.Q. Feng, J.H. Yin, A new simplified Hypothesis B method for calculating consolidation settlements of double soil layers exhibiting creep, Int. J. Numer. Anal. Methods GeoMech. 41 (6) (2017) 899–917.

[45] D. Nash, S. Ryde, Modelling consolidation accelerated by vertical drains in soils subject to creep, Geotechnique 51 (3) (2001) 257–273.

[46] J. Kruger, A. du Plessis, G. van Zijl, An investigation into the porosity of extrusion-based 3D printed concrete, Addit. Manuf. 37 (2021), 101740.